Design and Testing of a Four-Phase Fault-Tolerant Permanent-Magnet Machine for an Engine Fuel Pump

Barrie C. Mecrow, *Member, IEEE*, Alan G. Jack, *Member, IEEE*, David J. Atkinson, Simon R. Green, Glynn J. Atkinson, *Member, IEEE*, Andrew King, and Brian Green

***Abstract*—This paper discusses the design and testing of an aircraft electric fuel pump drive. The drive is a modular, four-phase, fault-tolerant system which is designed to meet the specification with a fault in any one of the phases. The motor employed has a permanent-magnet rotor with the magnets arranged in a Halbach array to maximize the air-gap flux density. Exceptionally high electric loadings are obtained by flooding the entire motor with aircraft fuel, which acts as an excellent cooling agent. Theoretical results are compared with test results gained in conditions approaching those found in an aircraft. Tests are carried out on the unfaulted drive and with one of several fault scenarios imposed. The electrical and thermal performance of the drive is assessed, showing how the flooded fuel cooling has excellent performance without introducing significant drag on the rotor.**

***Index Terms*—Aerospace industry, electromagnetic (EM) performance, fault tolerance, high specific output, permanent-magnet (PM) machines, testing.**

I. Introduction

THIS WORK discusses the design and testing of an aircraft electric fuel pump drive. The drive, which is flooded with aircraft fuel, must supply 16 kW of mechanical output power at 15 000 r/min. Two strands of research have been followed in earlier work: some researchers have concentrated on fault-tolerant switched reluctance machines (SRMs) [1]–[5], while other works have focused on permanent-magnet (PM) machines [6]–[8]. A PM machine is chosen in preference to a SRM [6] because the drive can be smaller and yet is equally fault tolerant. A very high magnetic loading is combined with the excellent cooling properties of the aircraft fuel to produce a very high specific output machine. In order to meet reliability requirements, the drive is fault tolerant; four independent modular phases are used, with the drive capable of meeting the specification when any one of the phases is faulted.

An earlier work [8] described a six-phase demonstrator which uses a similar modular design philosophy, how it detects faults [9], and how it continues to operate in the presence of open- and short-circuit faults or when a power device fails [10]. This paper describes the four-phase drive, which is a refinement of the earlier work; for the first time, a fault-tolerant fuel pump drive is operated in conditions approaching those in an aircraft, revealing thermal performance and capacity to deal with likely failures.

It has been shown how drives of this type can give rise to large rotor eddy current losses due to asynchronous magnetomotive-force (MMF) harmonics [11]. Extensive test results are presented (both using a dynamometer and driving the fuel pump), giving an insight into the electromagnetic (EM) and thermal performance of the fuel cooled machine under unfaulted and faulted load conditions.

II. Demonstrator Machine

The demonstrator machine uses the now well-established technique of making each phase of the machine an independent module with magnetic, electric, thermal, and mechanical isolation between modules. It is perhaps most appropriate to consider the complete drive as a collection of separate single-phase drives, rather than a combined multiphase structure. Mutual coupling between phases is minimized by having only one phase winding per slot, (thereby removing cross-slot mutual coupling) and maintaining deep magnets thereby virtually eliminating mutual coupling via the rotor. Windings are placed around every other tooth, giving mechanical and thermal isolation between phases, and each phase is supplied from a single phase bridge, giving electrical isolation between phases. Short circuits are accommodated by deliberately creating a per–unit inductance equal to that of the back emf, so that in the event of terminal short-circuit faults, the fault current is limited to rated value by the inductance. Internal winding faults are detected through the associated parameter changes creating increases in the pulsewidth-modulation (PWM) ripple current and are dealt with by deliberately shorting the faulted phase via the power converter.

Earlier work has concentrated on a six-phase drive: that drive was capable of producing rated output with only five phases operational and, therefore, had to be overrated by 20%. In contrast, the four-phase drive (in which each phase is separated by 90 electrical degrees) must operate with only three phases operational and must be overrated by 33%. However, the power electronics are considerably less complex, with two-thirds the number of power-electronic devices. The lower component count actually makes the drive more reliable in addition to making the power electronics smaller and lower cost. The space

Manuscript received June 20, 2003. Paper no. TEC-00087-2003.

B. C. Mecrow, A. G. Jack, D. J. Atkinson, and G. J. Atkinson are with the University of Newcastle upon Tyne, Newcastle upon Tyne NE1 7RU, U.K. (e-mail: Barrie.Mecrow@ncl.ac.uk).

S. R. Green is with Eurotherm Drives Ltd., Worthing, West Sussex, BN13 3PL, U.K.

A. King and B. Green are with Goodrich Engine Control Systems, Birmingham B28 8LN, U.K.

Digital Object Identifier 10.1109/TEC.2004.832074

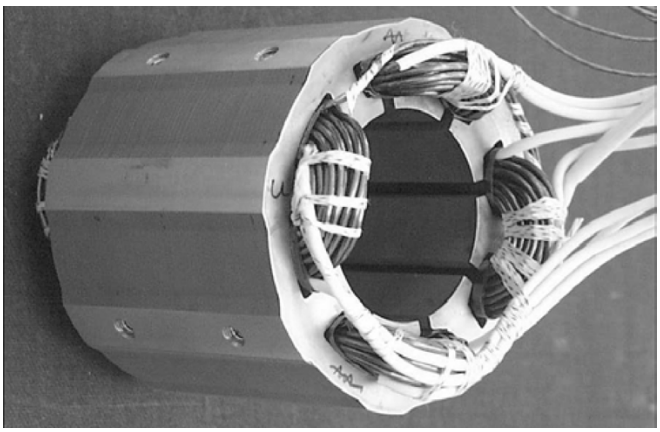

Fig. 1. Four-phase stator.

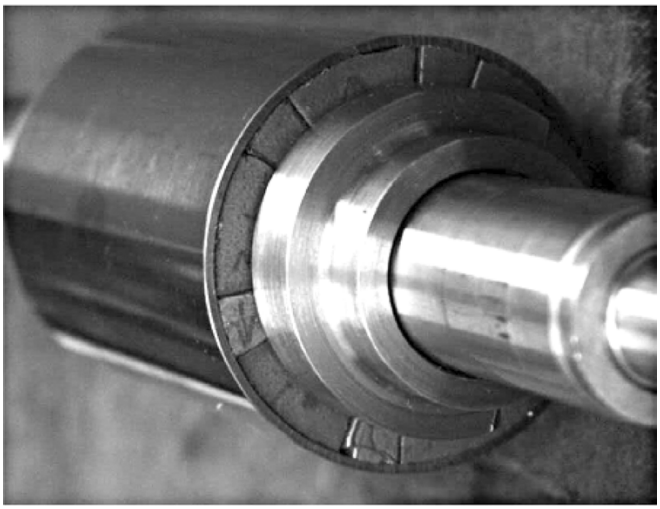

Fig. 2. Six-pole Halbach array rotor.

and weight of the power electronics are often ignored but, in fact, can be substantial. At this time, tightly packaged power electronics have yet to be developed, but choosing a lower phase number was heavily influenced by these considerations. Ultimately it was decided that the four-phase drive was the most attractive option, taking size, reliability, and complexity into account.

After choosing the phase number, there are a large number of choices which can be made for pole and teeth number. The speed of the machine is dictated here by the pump. The pump is of the gear type and 15 000 r/min is a rather high speed for such a pump. The drive needs to maintain full control and, hence, the operating frequency of the power electronics sets limits on the possible pole number. These arguments tend to favor a relatively low pole number which, in turn, limits the possible choices for the stator slotting arrangements. The four-phase drive described here has four coils, wound round four of the eight teeth, and six rotor poles. The stator, shown in Fig. 1, is constructed from 0.2–mm-thick cobalt-iron laminations, which combine a high magnetic flux density with a low iron loss. It has an outside diameter of 86 mm and a lamination stack length of 73 mm.

The rotor, shown in Fig. 2, contains samarium cobalt magnets, arranged in a Halbach array: This results in a significantly greater air-gap flux density than has been achieved with earlier

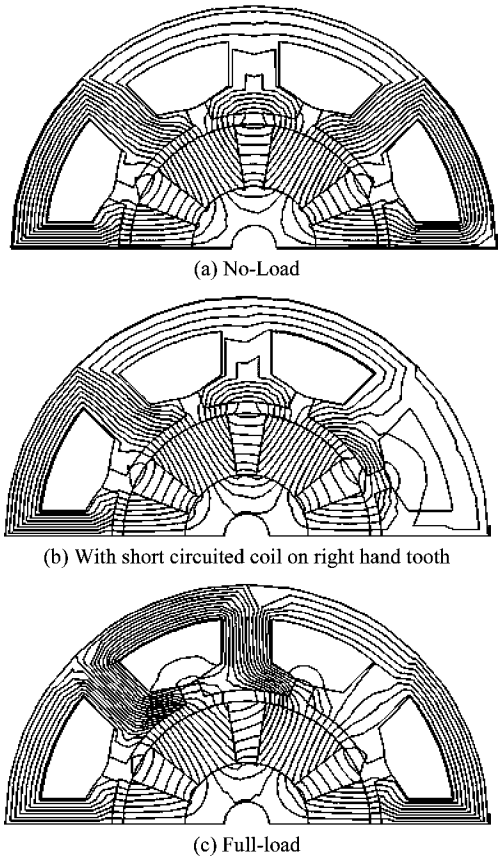

Fig. 3. Magnetic flux distribution in the four-phase machine.

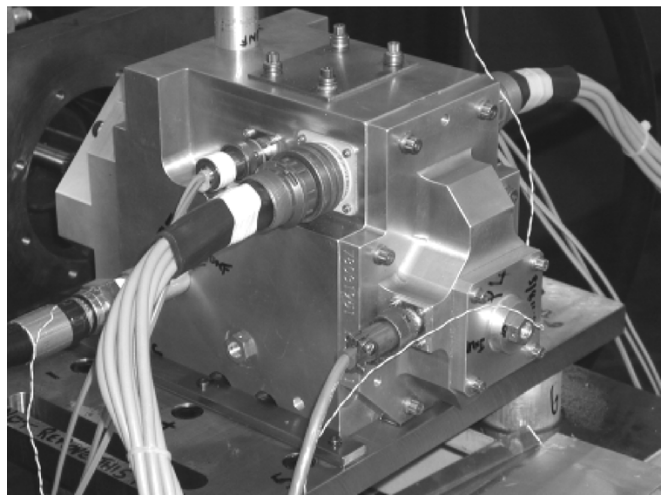

Fig. 4. Assembled machine on the dynamometer.

surface-mounted magnet designs. Samarium cobalt magnets are used because of their tolerance to temperature.

Fig. 3 shows the magnetic flux distribution in the machine on no-load, full-load, and with a single-phase short circuit. Phase coils are placed around the vertical and horizontal teeth, and so for the rotor position shown, there is peak-induced voltage in the coil round the vertical tooth. If the right-hand coil is shorted, then it produces peak demagnetizing MMF at this position, but note how the demagnetizing flux of (b) does not affect the flux linking of the other phases. On load there is peak MMF in the

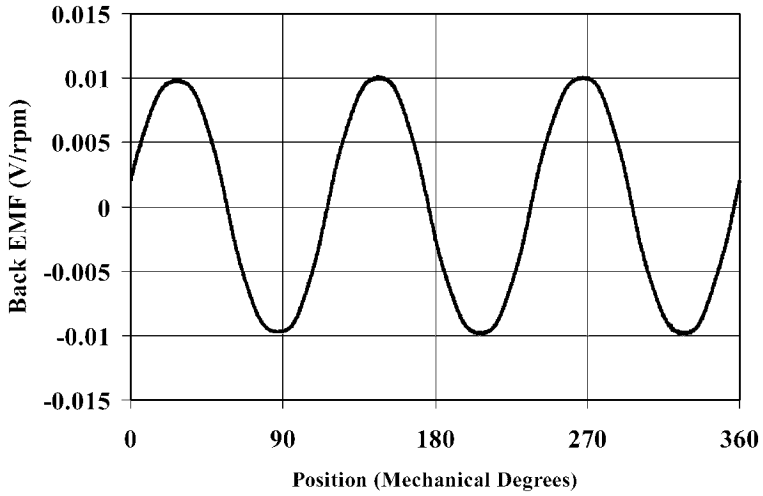

Fig. 5. Measured back emf waveforms in the four-phase motor.

phase wrapped around the vertical tooth and the resulting armature reaction field is clearly visible in the stator field. The air-gap field, however, is relatively unaffected by armature current and even when a winding is short circuited, the air-gap flux falls by less than 20%. This is a natural consequence of the deep magnets and the relatively large air gap which restricts the flux driven by the armature currents that reaches the rotor. This means that the magnets are never in danger of demagnetization by a fault, even in the zones near to the slot openings on the magnet surface. It also means that the unbalanced magnet pull caused by a fault is rather small. In fact, tests show that when short circuits are deliberately applied, the acoustic emissions from the motor hardly change, a clear indication of a benign vibration environment.

III. Dynamometer Test Rig

The assembled test motor, mounted on the dynamometer, is shown in Fig. 4. The motor has been run on two rigs: the first is a dynamometer using a dc load machine via a gear box and torque transducer, the second is a full fuel system rig with the motor integrated with its pump, fuel system, and controls. For safety reasons, the machine, while being tested on the dynamometer, used a very low viscosity oil to replace the fuel. This slightly impairs the cooling because the oil has a slightly higher viscosity than the fuel but the testing shows the difference to be very small. In this paper, the majority of the results come from the dynamometer testing because a full range of electrical tests is far easier to accomplish. The dynamometer results are presented in this section and a sample from the fuel system results is presented in Section VI.

Oil is pumped into the machine at the driving end, with the outlet pipe on the top of the motor, also at the driving end. The oil passes through the machine by two routes: one through the air gap, which is 1 mm deep, and a second through ducts formed in the laminations between the core back and frame (as may be seen in Fig. 1).

IV. Motor Characteristics

The motor back emf characteristics are shown in Fig. 5. The waveshape is virtually a pure sinusoid, as expected. Halbach array rotors tend to give a very good sinusoidal air-gap flux waveshape, leading to a sinusoidal back emf and this machine is no exception.

Measurements of the phase self and mutual inductances indicated that each phase has effectively 1.0-p.u. phase inductance, that the mutual inductance between adjacent phases was 0.028 p.u. and that between opposite phases was 0.018 p.u. This level of mutual coupling was so low that faults in a phase had no measurable effect upon the control and torque produced by any other phase.

An increase of 10% in self inductance was measured when compared to the theoretical phase inductance calculated using two-dimensional finite-element (2-D FE) methods, as shown in Fig. 3. Further investigation using three-dimensional (3-D) FE methods indicates that extra flux linkage due to the end windings account for this increase in inductance.

Because each phase is more or less independent of all others, each phase can be characterized by its own flux-linkage/current/position curves. These were measured in a two-stage process, first measuring the flux linkage due to the magnets and second measuring that due to the winding. Integrating the back emf with respect to time gives the no-load magnet flux. The variation of flux with current is then produced using a locked rotor test. The rotor is locked in different positions and a voltage pulse is applied to the winding. The resulting current versus time curve allows the flux linkage to be calculated. The two results are then summed together to produce the curves shown in Fig. 6.

To put these results into perspective, the machine running at its rated torque and speed reaches a peak current of 76 A. This shows that the motor is driven close to saturation and reaches most of the available flux linkage-current space (i.e., it is quite close to its EM limit).

V. Motor Tests

The machine has several thermocouples built into the stator slots and end windings. Temperatures were also measured at the oil inlet and outlet.

By maintaining a constant flow rate and measuring the difference between the oil inlet and outlet temperatures, the power

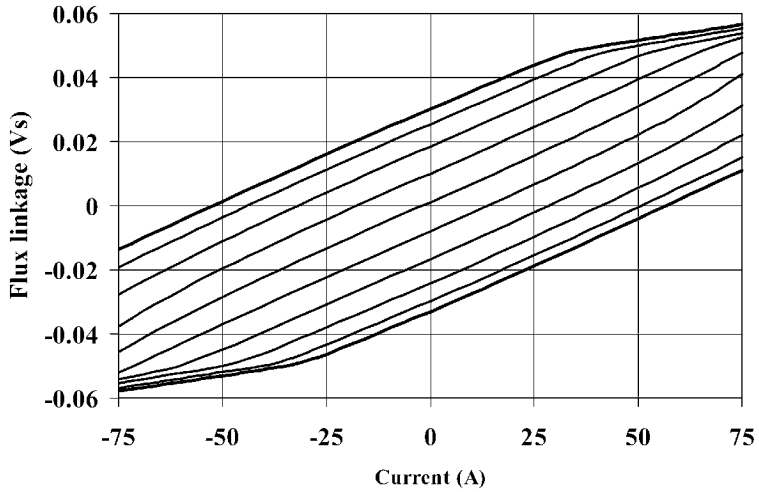

Fig. 6. Flux linkage/current for the four-phase machine. Each curve represents one rotor position from the magnet-aligned position = 0 electrical degrees (top curve) to 180 electrical degrees (bottom curve) in steps of 20 electrical degrees.

TABLE I
MEAN AND PEAK TEMPERATURE RISES OF THE MACHINE WHILE OPERATING AT 13 000 r/min. MEASUREMENTS TAKEN IN THE SLOT, THE END WINDING, AND THE OIL

Operating mode	Torque	Mean temperature rise (°C)			Peak temperature rise (°C)	
	(Nm)	Slot	End winding	Oil	Slot	End winding
Normal	2.13	4.5	3.75	4.0	5	5
	4.24	8.5	6.75	7.0	10	9
	6.33	13.0	8.75	8.0	15	12
Open circuit Winding Fault	2.18	8.0	6.75	7.0	12	10
	4.15	11.0	9.00	9.0	16	13
	5.98	14.0	11.25	11.0	21	17
Short Circuit Winding Fault	2.25	11.5	7.00	6.0	10	11
	4.26	14.0	8.25	9.0	15	11
	6.03	17.0	10.25	10.0	20	15

dissipated into the oil can be calculated. A series of tests was carried out using this method to find the loss produced by various mechanisms. It is assumed that the majority of loss is dissipated into the oil as its cooling effect is many times greater then the air surrounding the motor case and the associated mountings.

A. Winding Loss

With the rotor locked, a dc current was passed through all four phases and the temperature rise was measured. The winding temperature rise was found to be 0.014 °C/W, an exceptional thermal performance for such a small machine.

Repeating this test with only one phase reveals no detectable temperature rise in the adjacent or opposite phases. This is important as it illustrates the excellent thermal isolation between the phases, an important factor in reducing the propagation of any fault through the machine.

At full-load current in the unfaulted mode [equivalent to 38 A root mean square (rms) and 10.2 Nm], the dc winding loss is 395 W while running in the faulted mode (the highest loss mode) based on these dc tests would give 670 W of (dc) winding loss.

B. No-Load Loss

While open circuited, the machine is driven by a dc machine. Measuring the oil temperature rise gives an indication of no-load loss. As a dummy rotor was unavailable, the no-load loss measured is actually iron loss, generated by the rotation of the magnets, plus viscous drag and bearing loss. At 13 000 r/min, 549 W was dissipated into the oil. This may be compared with the dc I^2R loss above to reveal that the no-load losses are slightly smaller than the copper loss. It can also be seen that the viscous friction drag caused by running the rotor at high speed immersed in the oil is not very large.

C. Full-Load Operation

The drive has been extensively tested on the dynamometer up to a maximum speed of 13 000 r/min (set by the capability of the gear system on the dynamometer) and a range of torques, both during unfaulted and faulted operation. During normal operation, a peak temperature rise of 15 °C has been measured, even under fault conditions at rated torque, the peak temperature rise has not exceeded 25 °C. This is truly exceptional for a machine of this size. The specific output is 38 MWm^{-3}, which results from a combination of moderately high speed, a high magnetic loading, and very high electric loading, with rms current densities in excess of 25 A per square millimeter. Table I illustrates the mean and peak temperature rises at various locations throughout the machine, while Table II illustrates the com-

TABLE II
MACHINE LOSS COMPONENTS WHEN OPERATING AT 13 000 r/min

Operating mode	Torque (Nm)	No-load Loss (W)	Copper Loss (W)	Oil ΔT (°C)	Power dissipated into oil (W)	Extra loss (W)
Normal	6.33	549	296	8	1096	251
Open Circuit Fault	5.98	549	394	11	1507	564
Short Circuit Fault	6.03	549	502	10	1370	319

ponents of loss causing these temperature rises when operating at 13 000 r/min, the maximum test speed under fault conditions.

These temperature rises are probably lower than might be allowed in the full application, and hence, the machine could be produced a little smaller for the same output by reducing the copper cross-section, and hence, slot area and outside diameter without affecting the EM envelope (which, as has been shown in Section IV, is close to being fully utilized). The considerations on allowable temperature rise are related to ambient fuel temperature and to the power-electronics packaging and its temperature limit. In the prototype, the electronic circuits are entirely separate and air cooled but in a full implementation, it is intended that the electronics be packaged with the motor and fuel cooled. This is likely to impose a lower allowable temperature rise.

The distribution of temperature shows that the primary cooling path for the copper loss is out through the end windings which are fully immersed in moving coolant. The thermal gradients are small, which reduces problems associated with thermal cycling.

The measured total losses estimated from oil inlet and outlet temperatures are shown in Table II. The results display the no-load loss, the dc copper loss (according to the actual running condition), the total measured loss, and the "extra loss" which is the difference between the dc copper loss plus the no-load loss and the total loss. It should be noted that the oil temperature rises are small (with a maximum rise of only 11 °C), and hence, the likely level of error in these measurement is high. As with the temperature results, the fault modes give the highest losses. The figures also show that total running losses are substantially higher than the combination of dc copper loss and the no-load loss. The extra loss comes partially from the higher fluxes in the core resulting from the addition of the armature driven flux to the magnet flux and partially from the ac resistance of the windings. The other source of extra loss comes from the nonsynchronous magnetic fields produced by the winding which cause induced eddy currents in the rotor sleeve, magnets, and shaft.

During a fault, the healthy phase currents must increase (to maintain torque): this contributes extra winding loss—296 W rises to 394 W during an open-circuit phase fault and 502 W with a short-circuit phase fault because during a short-circuit fault, the faulted phase current will also contribute extra loss.

Rotor loss is due to eddy currents induced by asynchronous air-gap rotational fields. During normal operation, the rotor is only exposed to rotating odd harmonics; however, during faulted operation, the increased healthy phase currents increase the magnitude of the odd harmonics and the unbalanced nature

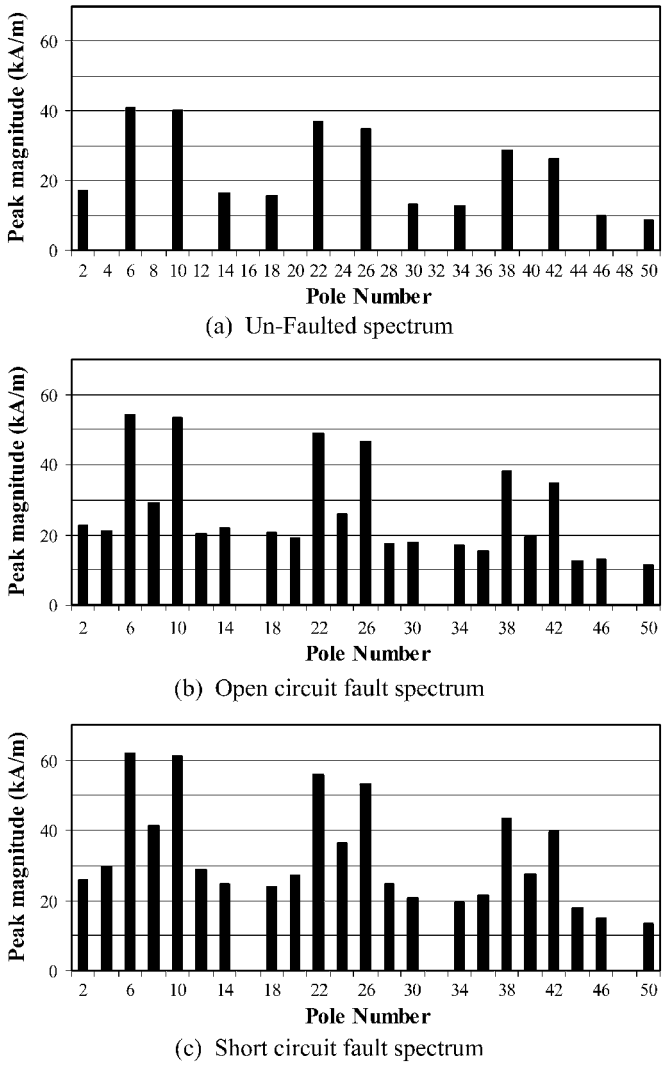

Fig. 7. Air-gap field harmonic spectrum during normal operation (top) and a short circuit fault (bottom).

of the air-gap field creates loss inducing even harmonics. These have been calculated using Fourier analysis of the predicted tangential H field at the stator bore. Fig. 7 illustrates the change in the air-gap harmonic spectrum during unfaulted, open-circuit, and short-circuit operation. In considering this figure, it should be noted that the harmonics are given as the tangential magnetic field strength appearing at the air gap with the units of kiloamperes per meter.

Displaying field strength as opposed to MMF means that the higher harmonics do not diminish as much as is instinctively expected. The magnet has a six-pole field and the winding's

TABLE III
SIMULATED ROTOR LOSS DURING NORMAL AND FAULTED OPERATING CONDITIONS

Operating mode	Simulated rotor loss (W)	Rotor loss (Per unit)
Normal	267	1.00
Open circuit fault	369	1.38
Short circuit fault	445	1.67

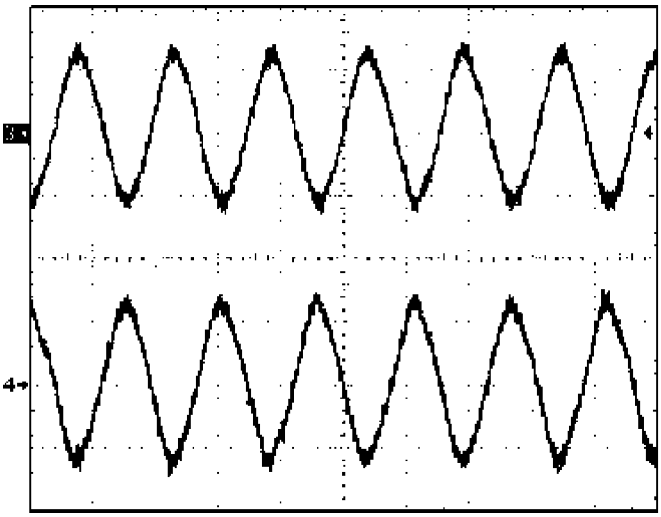

Fig. 8. Current in phases A and C when delivering 8.1 Nm at 13 000 r/min. Unfaulted operation (1 mS/div, 50 A/div).

six-pole field rotates with the rotor and creates the load torque. The other pole-numbered fields rotate either forward or backward at varying speeds nonsynchronous with the rotor and create loss via the induced eddy currents in the rotor.

Using a mix of Fourier methods and 2-D finite elements, the air-gap field is decomposed into its harmonic components, which are used to calculate rotor loss due to induced eddy currents. The results are shown in Table III. These calculated figures are in broad agreement with the measured extra loss considering the likely measurement errors. They also agree rather closely with another published work [11].

The measured figures for the extra loss certainly support the assertion that most of this extra loss is rotor eddy current loss. If the extra loss was all rotor eddy currents, the short-circuit fault case should have lead to substantially more loss than the open-circuit fault. A possible explanation why this is not the case is that the open-circuit case has full flux in the faulted phase, and hence, the iron loss associated with that, whereas the short-circuit phase has no linking flux, and hence, negligible iron loss in that part of the magnetic circuit. It should be remembered that the oil temperature rises are small, and hence, the error level will be high.

Fig. 8 shows the measured phase currents during normal operation at 13 000 r/min with 8-Nm torque, while Fig. 9 shows the currents during faulted operation at 6 Nm.

In this case, phase C, the lower trace, is short circuited at the terminals. The figure illustrates how the fault current remains

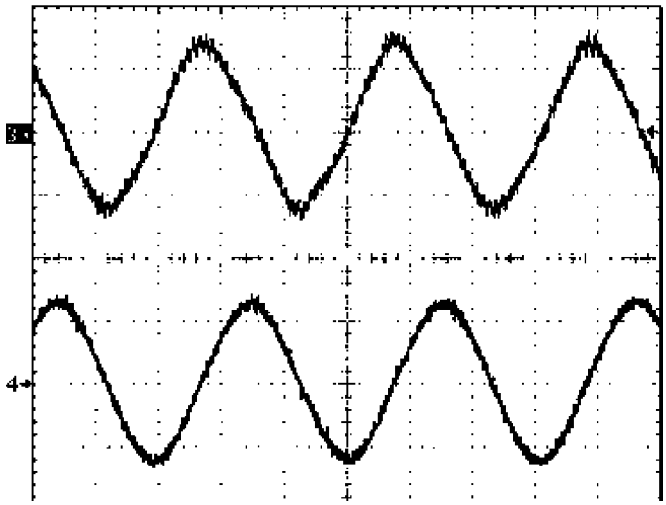

Fig. 9. Current in phases A and C when delivering 7.1 Nm at 13 000 r/min. Phase C (lower trace) is subject to a short circuit with all torque produced by phases A, B, and D (500 μS/div, 50 A/div).

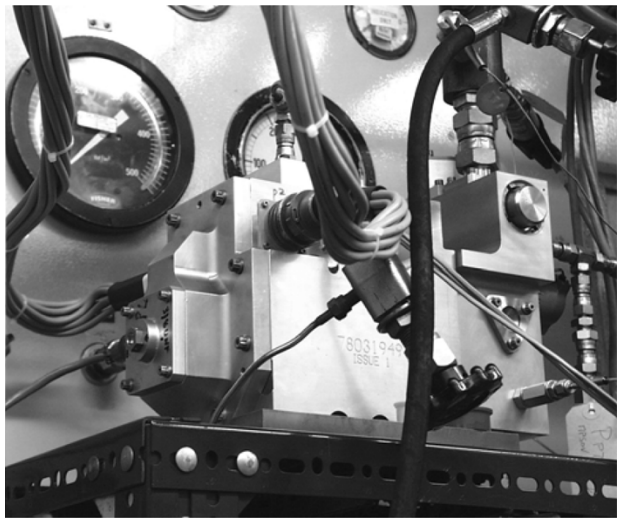

Fig. 10. Full motor and pump system test rig.

within the rated value and that of phase A is unaffected by the fault.

VI. TESTING OF THE DRIVE WITH THE PUMP

After thorough testing of the drive on the dynamometer, the machine was mated with its pump and full system tests conducted. Detail of the test rig is shown in Fig. 10. The machine is identifiable on the left of the picture with the pump and its fuel connections on the right.

These tests were conducted in actual fuel, as opposed to the low viscosity oil that was used in replacement of jet fuel in the dynamometer tests. The pump, which is of the gear type, was driven over a range of operating conditions both with and without faults imposed. A full description of the pumping system is beyond the scope of this paper but perhaps Figs. 11 and 12, which show results from normal operation during a speed increase from 11 900 to 12 800 and operating through temporary loss of a phase, serve to illustrate performance.

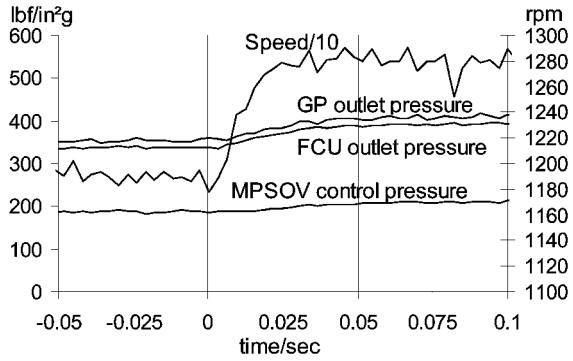

Fig. 11. Acceleration of the pump from 11,900 to 12 800 r/min with the maximum acceleration rate set at 100 000 r/min/s.

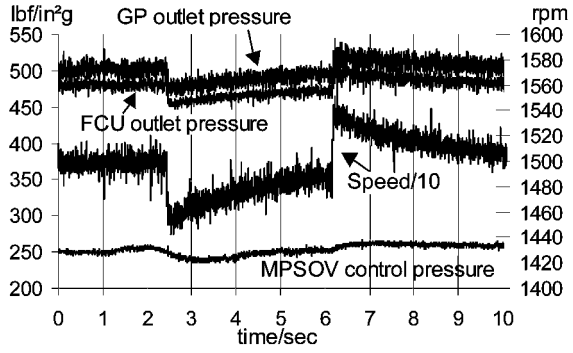

Fig. 12. Pump running at 480 1 $\mathrm{b/in^2g}$ (15 000) r/min set point running through temporary loss of a phase.

In these figures, GP outlet pressure is the pressure directly at the output of the (gear) pump, FCU outlet pressure is the pressure at the outlet from the fuel control unit, speed/10 is one-tenth the speed of the pump, and MPSOV control pressure is the pressure at the minimum pressure shutoff valve, used to prevent overheating of the machine if the fuel pressure falls below a minimum value.

During the pump tests, the speed was controlled by the MPSOV control pressure measurement, as seen above in Fig. 12. This method slows down the speed response of the drive. The scale in Fig. 12 has a truncated zero and the actual speed changes are small and well within acceptable limits. The drive runs its own fault detection, and hence, is able to autonomously correct the required target current for a given torque demand. Using this would result in faster response to more or less at the same rate as the current controller. This action was not employed in these tests as full integration of the pump and motor controllers has yet to be implemented.

It should be noted that these full pump tests have been performed at full-rated speed and torque (as compared with the 13 000-r/min restriction placed on the dynamometer tests).

VII. Conclusion

A four-phase fault-tolerant fuel pump drive has been designed, built, and extensively tested. The drive has demonstrated its ability to continue to produce rated output, even in the presence of faults to the machine.

Through the use of Halbach magnets and fuel cooling, an exceptionally high specific output has been achieved for the machine. The temperature rises measured in the drive are very modest even during faulted operation. This indicates some scope for further improvement in specific output.

It has been possible to assess the various loss mechanisms present in the machine which has shown that the running losses due to iron loss, rotor eddy current loss, and viscous drag of the fuel are all significant. The highest temperatures are reached during faulted operation during which the healthy phases must carry higher current and there are extra losses caused by the increase in rotor eddy currents driven by extra nonsynchronous fields arising from the nonsymmetric armature currents during the fault. None of these loss mechanisms led to excessive temperature rise during a fault.

Tests have been conducted with the drive integrated with a fully functional pump and the associated pump control valves. Excellent performance has been shown in these full running tests including ride through performance during an imposed fault in the drive.

The tests to date fully justify the design methodology adopted to create a fault-tolerant electric drive for a main engine fuel pump using a modular redundant PM machine-based drive.

References

[1] E. Richter, "Switched reluctance machines for high performance operations in a harsh environment—A review paper," in *Proc. Int. Conf. Electrical Machines*, Boston, MA, 1990.

[2] A. V. Radun, "High power density switched reluctance motor drive for aerospace applications," *IEEE Trans. Ind. Applicat.*, pt. 1, vol. 28, pp. 113–119, Jan./Feb. 1992.

[3] T. J. E. Miller, "Faults and unbalanced forces in the switched reluctance machine," *IEEE Trans. Ind. Applicat.*, vol. 31, pp. 319–328, Mar./Apr. 1995.

[4] C. M. Stephens, "Fault detection and management system for fault-tolerant switched reluctance motor drives," *IEEE Trans. Ind. Applicat.*, vol. 27, pp. 1098–1102, Nov. 1991.

[5] A. A. Ferreira, S. R. Jones, B. T. Drager, and W. S. Heglund, "Design and implementation of a five-hp switched reluctance, fuel-lube, pump motor drive for a gas turbine engine," *IEEE Trans. Power Electron.*, vol. 10, pp. 55–61, Jan. 1995.

[6] T. M. Jahns, "Improved reliability in solid state a.c. drives by means of multiple independent phase-drive units," *IEEE Trans. Ind. Applicat. Soc.*, vol. IA-16, pp. 321–331, May 1980.

[7] A. G. Jack, B. C. Mecrow, and J. Haylock, "A comparative study of permanent magnet and switched reluctance motors for high performance fault tolerant applications," *IEEE Trans. Ind. Applicat.*, vol. 32, pp. 889–895, July/Aug. 1996.

[8] B. C. Mecrow, A. G. Jack, and J. A. Haylock, "Fault tolerant permanent magnet machine drives," *Proc. Inst. Elect. Eng. B*, Nov. 1996.

[9] J. A. Haylock, B. C. Mecrow, A. G. Jack, and D. J. Atkinson, "On-Line detection of winding short-circuits in inverter fed drives," in *Proc. 9th Int. Conf. Elect. Mach. Drives*, Canterbury, U.K., Sept. 1–3, 1999, pp. 258–262.

[10] ——, "Operation of fault tolerant machines with winding failures," in *Proc. IEEE Int. Electric Machines Drives Conf.*, Milwaukee, WI, 1997.

[11] J. D. Ede, K. Atallah, J. B. Wang, and D. Howe, "Modular fault-tolerant permanent magnet brushless machines," in *Proc. Inst. Elect. Eng. Int. Conf. Power Electronics, Machines Drives*, 2002.

Barrie C. Mecrow (M'98) is a Professor of electrical power engineering with the University of Newcastle upon Tyne, Newcastle upon Tyne, U.K., where he has been since 1987. He was a Turbogenerator Design Engineer with NEI Parsons, Newcastle upon Tyne, until 1987. He is involved in a range of research projects, including fault-tolerant drives, high-performance permanent-magnet (PM) machines, and novel switched reluctance drives.

Alan G. Jack (M'00) received the Ph.D. degree for work on numerical analysis of electromagnetic (EM) fields in turbogenerators from Southampton University, Southampton, U.K., in 1975.

He is past head of the department and leader of the Newcastle Electric Drives and Machines Group at the University of Newcastle upon Tyne, Newcastle upon Tyne, U.K. He has been with Southampton University for more than 20 years, joining them from NEI Parsons, Newcastle upon Tyne, whom he was with for 13 years with roles from Craft Apprentice to Principal Design Engineer. He is the author of more than 80 papers in the area of electrical machines and drives. He holds the Department's Chair in electrical engineering.

David J. Atkinson received the Ph.D. degree from The University of Newcastle upon Tyne, Newcastle upon Tyne, U.K., for research into the use of Kalman filter-based estimation on induction motor vector-controlled drives.

Currently, he is a Senior Lecturer in the Drives and Machines Group at the University of Newcastle. His research interests include electrical drive systems, real-time estimation and control, power electronics, and wind power generation. His research interests include sensorless vector drives, fault-tolerant drives, and cascade induction generators. Prior to his university appointment in 1987, he had spent 17 years in the industry.

Simon R. Green received the Ph.D. degree for work on sensorless control of permanent-magnet (PM) machines and control of unity power factor input on variable frequency supplies in a safety critical aerospace application from The University of Newcastle upon Tyne, Newcastle upon Tyne, U.K., in 2001.

Prior to joining The University of Newcastle upon Tyne in 1997, he was an Engineer for Eurostar UK Ltd., London, U.K., working on the commissioning and maintenance of Eurostar trains. In 2000, he joined Eurotherm Drives, Worthing, West Sussex, U.K., as a Design Engineer, primarily working in the area of induction motor control.

Glynn J. Atkinson (M'03) received the M.Sc. degree in electrical and electronic engineering at Newcastle University, Newcastle upon Tyne, U.K., in 2001, where he is currently pursuing the Ph.D. degree in engineering.

Currently, he is researching the design of fault-tolerant machines for use in aerospace applications.

Andrew King is with Goodrich Engine Control Systems Ltd., Birmingham, U.K., involved in research and development, looking at novel fuel system components and systems. His main project during this time has been the development of a more electric fuel system utilizing a switched reluctance drive, which was demonstrated on a Rolls-Royce Spey engine at the Defense Evaluation and Research Agency (DERA).

Brian Green received the B.Sc. degree in physics and electronic engineering and the M.Sc. degree in control engineering and computer systems from Leeds University, Leeds, U.K., in 1979 and 1982, respectively.

Currently, he is a Senior Principle Engineer with the Goodrich Electric Motor Drive Systems Technical Centre based at the Goodrich Engine Control Systems site, Birmingham, U.K. He also has a degree in high reliability software and hardware techniques. His areas of research and expertise are in engine control systems and flight actuation. He has more than 20 years of experience in various areas of the aerospace industry.